

A Practical Adaptive Proportional-Derivative Guidance Law

Yongwei Zhang, Min Gao, Suochang Yang, Baochen Li, Xue Gao

Abstract—The well-known proportional navigation guidance (PNG) often produces unwished guidance command for the entire flight so that big overload is needed. In this paper, we proposed a new adaptive proportional-derivative guidance (APDG) law for the guidance of mortar projectiles in the horizontal plane. An example trajectory and Monte Carlo simulations are simulated to verify the effectiveness of APDG. The result of the example trajectory and the Monte Carlo simulations indicates that the APDG is effective in eliminating error due to launch perturbations and atmospheric wind.

Index Terms—Guided mortar projectiles, proportional navigation guidance, adaptive proportional-derivative guidance

I. INTRODUCTION

FIRING accuracy of the guided projectiles can be dramatically improved by outfitting with a suitable trajectory correction system. The commonly used executive organs are impulse thrusters [1]-[2], drag brakes [3], inertial loads [4], and canards [5]-[7].

Research and development on the guidance and control of guided munitions has been going on for decades. Rogers has presented a design of a canard-controlled mortar projectile using a bank-to-turn concept. The smart mortar is equipped with a set of two reciprocating fixed-angle roll canards and a set of two reciprocating fixed-angle maneuver canards, and an active control system is designed to perform trajectory corrections. Monte Carlo simulations demonstrate that the control system is effective in reducing dispersion error [5]. Yi Wang has presented the correction control mechanism for a class of spin-stabilized projectile through studying the influence of correction to the dynamic equilibrium angle and attack angle [6]. Spagni has characterized the system equilibrium point manifold in terms of a minimal vector of scheduling variables for a class of reciprocating

canard-guided artillery munitions, giving rise to a discussion concerning the canard size and position for maneuverability optimization [7]. PNG is widely used in various types of guided munitions due to its computational simplicity [8], and many scholars have proposed a variety of modified forms of proportional navigation law for different needs or constraints [9]-[11]. However, the well-known PNG often produces unwished guidance command for the entire flight so that big overload is needed. In this paper, we proposed a new adaptive proportional-derivative guidance law for the guidance of mortar projectiles with canards.

The outline of the paper is as follows: Sec.II presents the trajectory model of the guided mortar projectile. Sec.III presents the adaptive proportional-derivative guidance law. Sec.IV describes the simulation result, and conclusion is provided in Sec.V.

II. MODELING

The schematic of the guided mortar is shown in Fig. 1. The projectile weight, mass center location from the nose tip, diameter, pitch inertia, and roll inertia is 15.0 kg, 0.387 m, 120 mm, $0.70 \text{ kg} \cdot \text{m}^2$, and $0.0261 \text{ kg} \cdot \text{m}^2$, respectively.

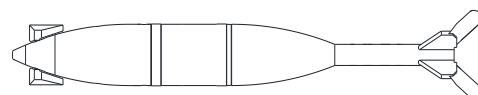


Fig. 1. Schematic of the guided mortar projectile

Fig. 2 shows schematic of forces on the guided mortar projectile. The forces applied on the guided mortar projectile including weight force and aerodynamic force. The deflection angle of canards is adjusted to change the aerodynamic force for trajectory correction in flight.

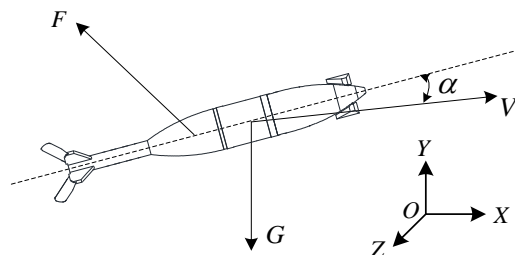


Fig. 2. Schematic of forces on the guided mortar projectile

In Fig. 2, α is the attack angle, G is the weight force, F is the aerodynamic force.

The numerical simulation is based on a rigid body six degree of freedom model typically utilized in flight dynamic

Manuscript received January 14, 2016.

Yongwei Zhang is with Electronic Engineering Department, Shijiazhuang Mechanical Engineering College, No.97 Heping West Road, Shijiazhuang, Hebei, 050003, China. (corresponding author, phone: 18911136093, e-mail: yongwei1112@sina.com).

Min Gao is with Electronic Engineering Department, Shijiazhuang Mechanical Engineering College, No.97 Heping West Road, Shijiazhuang, Hebei, 050003, China. (e-mail: gaomin1103@yeah.net).

Suochang Yang is with Electronic Engineering Department, Shijiazhuang Mechanical Engineering College, No.97 Heping West Road, Shijiazhuang, Hebei, 050003, China. (e-mail: yangsuochang_jx@sina.com).

Baochen Li is with Electronic Engineering Department, Shijiazhuang Mechanical Engineering College, No.97 Heping West Road, Shijiazhuang, Hebei, 050003, China. (e-mail: libaochen_jx@sina.com).

Xue Gao is with Baicheng Ordnance Test Center of China, Baichen, Jilin, 137001, China. (e-mail: gaoxue_jx@sina.com).

analysis of mortar projectiles [12]. The translational kinetic differential equations are given by

$$\begin{cases} \frac{dV}{dt} = G_{x_2} + F_{x_2} \\ V \frac{d\theta}{dt} = G_{y_2} + F_{y_2} \\ -V \cos \theta \frac{d\psi_v}{dt} = G_{z_2} + F_{z_2} \end{cases} \quad (1)$$

The applied forces in (1) consist of weight force (G), and aerodynamic force (F), expressed in aero-ballistic reference frame. V , ψ_v , and θ are the velocity, trajectory azimuth angle, and trajectory incline angle, respectively.

The rotational kinetic differential equations are given by

$$\begin{bmatrix} J_{x_4} \frac{d\omega_{x_4}}{dt} \\ J_{y_4} \frac{d\omega_{y_4}}{dt} \\ J_{z_4} \frac{d\omega_{z_4}}{dt} \end{bmatrix} = \begin{bmatrix} M_{x_4} + M'_{x_4} \\ M_{y_4} + M'_{y_4} \\ M_{z_4} + M'_{z_4} \end{bmatrix} - \begin{bmatrix} 0 \\ (J_{x_4} - J_{z_4})\omega_{x_4}\omega_{z_4} \\ (J_{y_4} - J_{x_4})\omega_{y_4}\omega_{x_4} \end{bmatrix} + \begin{bmatrix} 0 \\ -J_{z_4}\omega_{z_4} \frac{d\gamma}{dt} \\ J_{y_4}\omega_{y_4} \frac{d\gamma}{dt} \end{bmatrix} \quad (2)$$

The applied moments in (2) contain contributions from steady air loads, denoted by M , and unsteady air loads, denoted by M' , expressed in quasi-body reference frame. $J_{x_4}, J_{y_4}, J_{z_4}$ are components of the transverse moment of inertia. $w_{x_4}, w_{y_4}, w_{z_4}$ are components of the angular rate vector, γ is the Euler roll angle.

The translational kinematic equations are given by

$$\begin{cases} \frac{dx}{dt} = V \cos \theta \cos \psi_v \\ \frac{dy}{dt} = V \sin \theta \\ \frac{dz}{dt} = -V \cos \theta \sin \psi_v \end{cases} \quad (3)$$

Where x, y, z are position vector components of the center of mass, expressed in the inertial reference frame.

The rotational kinematic equations are given by

$$\begin{cases} \frac{d\vartheta}{dt} = w_{z_4} \\ \frac{d\psi}{dt} = \frac{1}{\cos \vartheta} w_{y_4} \\ \frac{d\gamma}{dt} = w_{x_4} - w_{y_4} \tan \vartheta \end{cases} \quad (4)$$

Where ϑ is the pitch angle, and ψ is the yaw angle.

The angles in (1) - (4) have the relation expressed in (5).

$$\begin{cases} \beta = \arcsin[\cos \theta \sin(\psi - \psi_v)] \\ \alpha = \vartheta - \arcsin\left(\frac{\sin \theta}{\cos \beta}\right) \\ \gamma_v = \arcsin(\tan \theta \tan \beta) \end{cases} \quad (5)$$

Where α is the attack angle, β is the sideslip angle.

Equations (1) - (5) constitute the rigid body six degree of freedom model for the guided mortar projectile, which can be solved by the fourth-order Runge-kutta algorithm.

III. METHODOLOGY

The motion relationship model of the projectile and target is established in the horizontal plane. As shown in Fig. 3, T is the target position, M is the projectile position, x_m and z_m are position vector components of the projectile, v_m is the projectile velocity, v_{xm} is the longitudinal velocity, and v_{zm} is

the horizontal velocity.

The APDG scheme is shown in (6).

$$\begin{cases} U_\sigma = k_p \cdot z_m + k_d \cdot v_{zm} \\ k_p = 1 \\ k_d = t_n - t \end{cases} \quad (6)$$

Where U_σ is the required overload in horizontal plane, t_n is the total flight time of the nominal trajectory, and t is the flight time. k_p is the proportional factor, which is set as 1 in this paper. k_d is the derivative factor, which is adaptive to the change of the flight time. The application progress of the APDG is shown in Fig. 4.

The application progress of the APDG is:

1) Ground computer calculates the nominal trajectory, and gets the total flight time t_n .

2) Operations personnel loads the total flight time t_n to the onboard computer.

3) The guidance system gets real-time derivative factor k_d through subtracting the real-time flight time t from the total flight time t_n of the nominal trajectory.

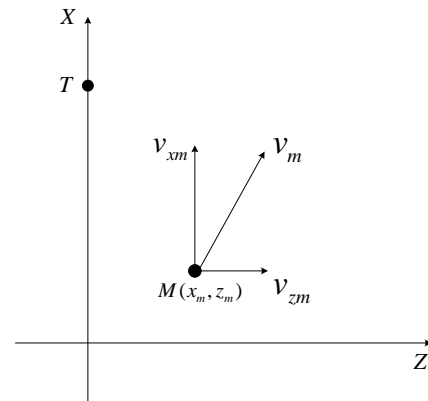


Fig. 3. Relation schematic between the mortar projectile and the target

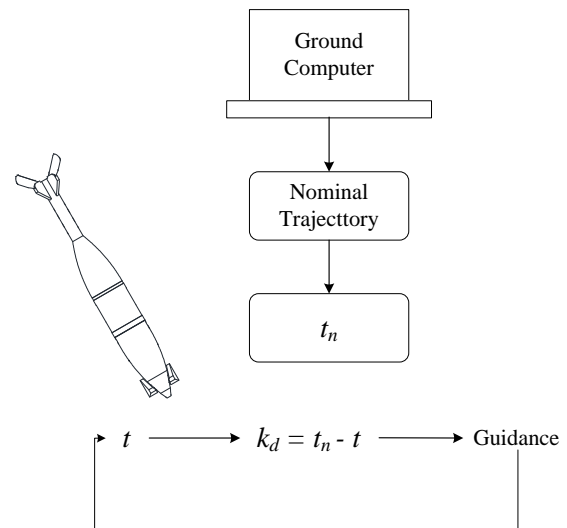


Fig. 4. Application process of APDG

The control method of the canards used in the guided mortar projectile is letting the deflection angle of canards follows a sinusoidal signal of the projectile roll angle, as shown in (7).

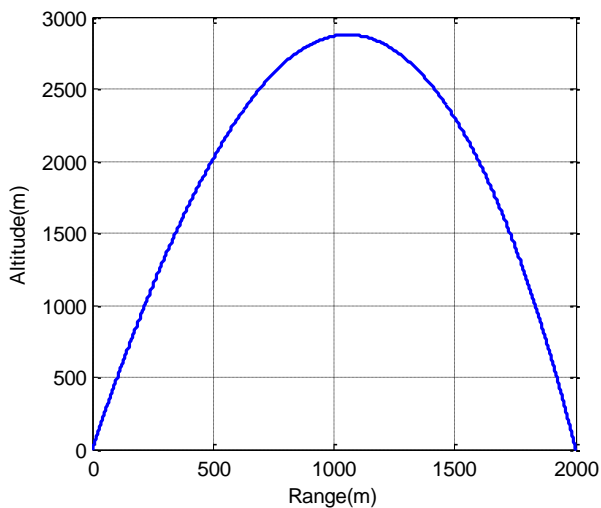
$$\begin{cases} \delta_i = \delta_0 \cdot \sin(\gamma + \pi/2 - \phi) \\ \delta_0 = k \sqrt{U_\sigma^2 + U_\theta^2} \\ \phi = \text{atan}(U_\sigma / U_\theta) \end{cases} \quad (7)$$

Where δ_i is the canards deflection angle, δ_0 is the amplitude of canards deflection angle, ϕ is the canards control phase, γ is the roll angle, k is coefficient, U_θ is the required overload in longitudinal plane.

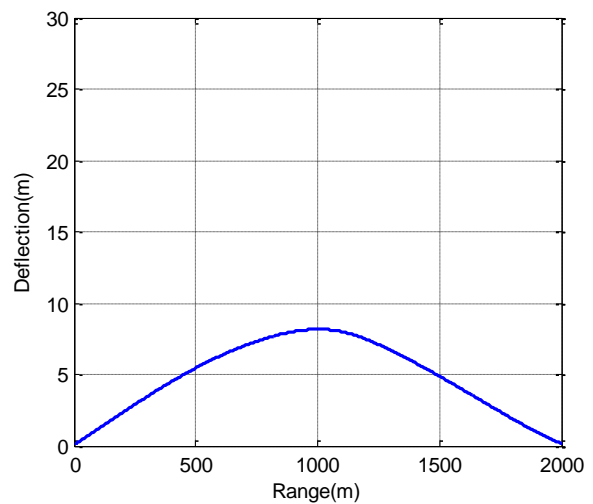
IV. SIMULATIONS AND DISCUSSION

A. Nominal trajectory

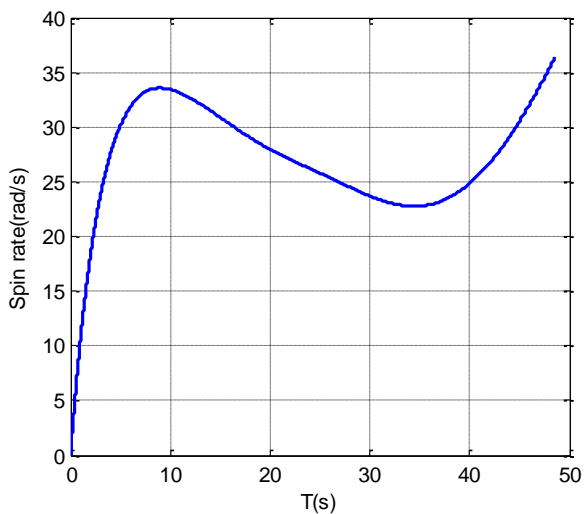
A nominal trajectory is simulated around which perturbations were studied. The launching elevation angle, launching azimuth angle, and initial velocity are 78.6 deg, -0.11 deg and 280 m/s, respectively. The trajectory, spin rate and velocity profile are presented in Fig. 5. The range of the nominal trajectory is 2000 m, and the cross range is 0 m with apogee at 2863 m. The spin rate changes at the range of 22.7 rad/s to 36.8 rad/s after 10 s. The velocity decreases gradually during 0 s to 22.4 s, gets the minimum value of 48.6 m/s, then increases gradually after 22.4 s, and the velocity before impact is 211 m/s.



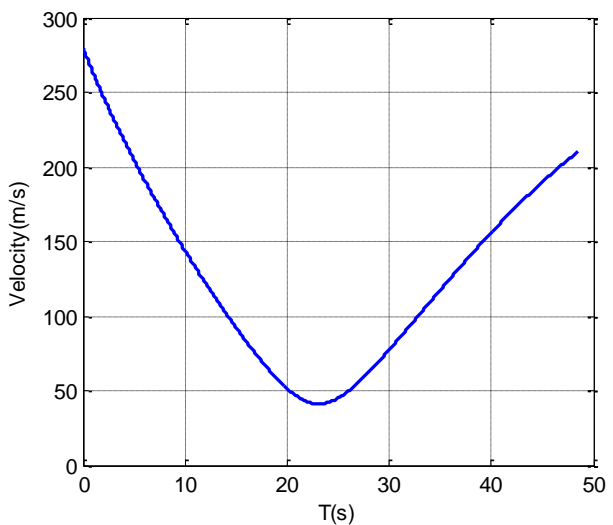
(a) Range vs. Altitude



(b) Range vs. Deflection



(c) Spin rate



(d) Velocity

Fig. 5. Nominal trajectory

B. Example Trajectory

An example trajectory is simulated to verify the effectiveness of APDG. The longitudinal plane is set as uncontrolled to stand out the trajectory performance of APDG in the horizontal plane. The control start time is set as 10 s. The uncontrolled trajectory and controlled trajectory are simulated using the perturbed value of initial conditions shown in Table I.

Fig. 6 shows the trajectory response obtained using the APDG. The figure shows an uncontrolled trajectory and an APDG controlled trajectory. The horizontal impact point error is 144.3 m in the uncontrolled case. Fig. 6 demonstrates that the APDG controlled trajectory is successful in reducing the horizontal impact point error, recording the controlled horizontal impact point error of less than 1 m, compared with the horizontal impact point error of 144.3 m for the uncontrolled case.

Fig. 7 plots the canards deflection histories of the controlled trajectory with APDG. The amplitude of canards deflection angle maintains at 15 deg during 10 s to 13.6 s, and reduces gradually after 13.6 s. The control phase maintains at 90 deg in most of time.

TABLE I INITIAL CONDITIONS FOR EXAMPLE SIMULATION

State	Unit	Unperturbed value	Perturbed value
Launching elevation angle	deg	78.6	78.6
Launching azimuth angle	deg	-0.11	-0.92
Initial velocity	m/s	280	280
Wind	m/s	0	2
Wind direction	deg	0	270

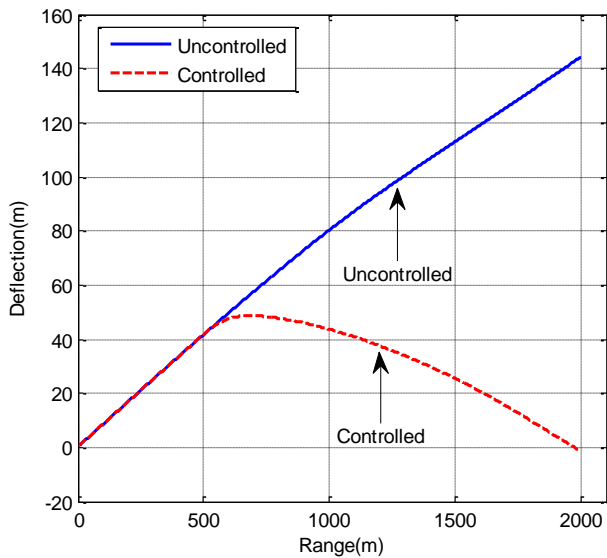


Fig. 6. Deflection vs. Range

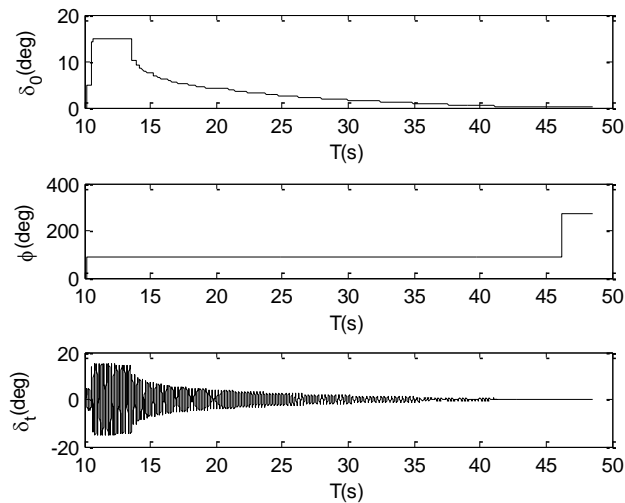


Fig. 7. The canards deflection histories with APDG

C. Dispersion Analysis

The robustness of APDG to handle initial errors and wind is studied by comparing the uncontrolled and controlled dispersions for individual errors and the combination of these errors. The nominal firing case described in Table I is used as reference. The initial azimuth angle errors and wind are added as perturbations. The azimuth angle errors are normally distributed with a standard deviation of 0.4 deg, and the wind is normally distributed with a standard deviation of 2.0 m/s.

200 Monte Carlo simulations are performed and presented below as dispersion plots for each studied set of error combinations. The results for standalone azimuth angle errors and wind are presented in Fig. 8 and Fig. 9 with statistics presented in Table II and Table III. The results for the combinations of errors are presented in Fig. 10 with statistics presented in Table IV.

TABLE II STATISTICS FROM 200 MONTE CARLO SIMULATIONS WHERE PERTURBATIONS ON WIND WERE ADDED

State	Uncontrolled		Controlled	
	Mean	Std. Dev.	Mean	Std. Dev.
Deflection (m)	-0.57	26.30	-0.88	5.10
Range (m)	2000.09	0.77	1999.81	0.71

TABLE III STATISTICS FROM 200 MONTE CARLO SIMULATIONS WHERE PERTURBATIONS ON AZIMUTH ANGLE WERE ADDED

State	Uncontrolled		Controlled	
	Mean	Std. Dev.	Mean	Std. Dev.
Deflection (m)	3.05	68.07	-1.21	5.51
Range (m)	2000.11	0.55	1999.93	0.44

TABLE IV STATISTICS FROM 200 MONTE CARLO SIMULATIONS WHERE PERTURBATIONS ON AZIMUTH ANGLE AND WIND WERE ADDED

State	Uncontrolled		Controlled	
	Mean	Std. Dev.	Mean	Std. Dev.
Deflection (m)	-6.15	71.86	-2.11	6.28
Range (m)	2000.05	0.98	1999.55	1.18

The impact point dispersion results from perturbations on azimuth angle errors and wind in Tables II-IV and figures 8-10 show a great decrease in the standard deviation of the deflection. From the impact point dispersion results it can be known that the APDG is effective in eliminating error due to launch perturbations and atmospheric wind.

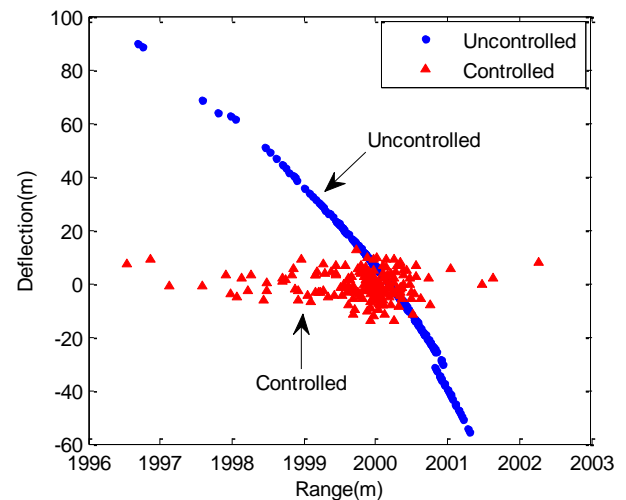


Fig. 8. Dispersion with wind

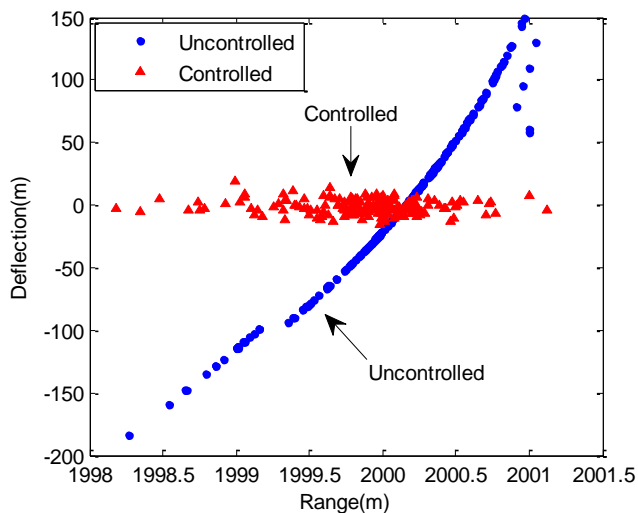


Fig. 9. Dispersion with azimuth angle errors

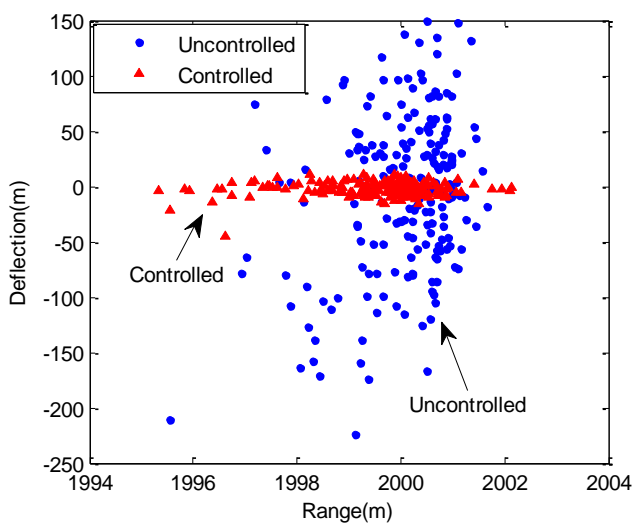


Fig. 10. Dispersion with azimuth angle errors and wind

To further analyze the expected accuracy of the proposed guidance law, the standard deviation of deflection was evaluated for a set of nominal elevation angles. In Fig. 11 the standard deviation of deflection is presented based on 100 Monte Carlo runs for each elevation angle. The azimuth angle errors and wind are normally distributed with a standard deviation of 0.4 deg and 2.0 m/s, respectively.

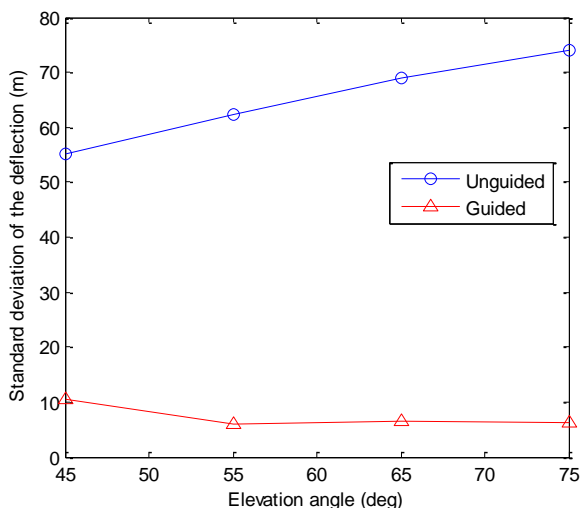
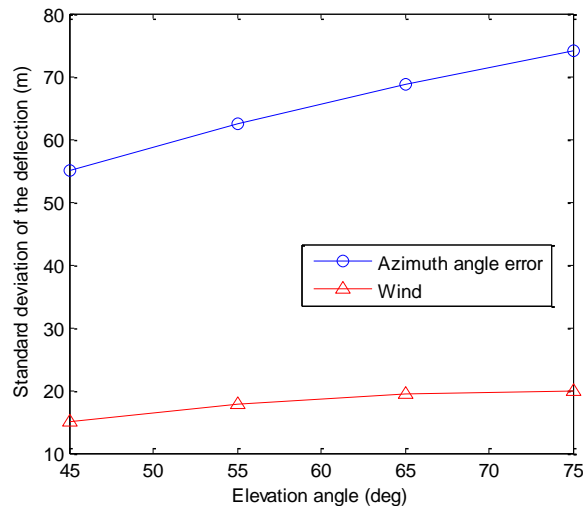
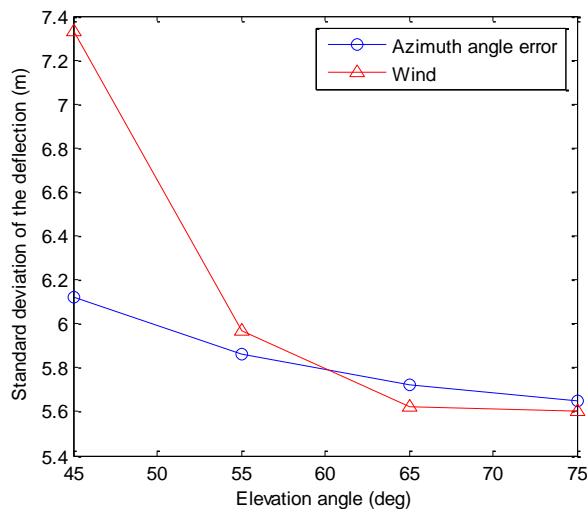


Fig. 11. Standard deviation of deflection as a function of elevation angle

As shown in Fig. 11, the effectiveness of the proposed guidance law is degraded for very low elevation angles. This can also be seen in Fig. 12 where the impact of the individual errors on the accuracy is displayed. The standard deviation of deflection for unguided mortar projectiles increases as the elevation angle increases, while the standard deviation of deflection for guided mortar projectiles decreases as the elevation angle increases. The results indicate that the proposed guidance law has better guidance performance for the large elevation firing cases.



(a) Unguided



(b) Guided

Fig. 12. Standard deviation as a function of elevation angle for standalone azimuth angle errors and wind

V. CONCLUSION

An APDG law is put forward for the guidance of the guided mortar projectiles in the horizontal plane in this paper. The horizontal velocity and horizontal position are taken as the control variables, and the derivative factor is adaptive to the change of the flight time. The simulation of an example trajectory was done to verify the effectiveness of the APDG. The Monte Carlo simulations indicate that the APDG is effective in eliminating error due to launch perturbations and atmospheric wind, and the proposed APDG has better guidance performance for the large elevation firing cases.

REFERENCES

- [1] Pavic M, Pavkovic B, Mandic S, Zivkovic S, and Cuk D, "Pulse-Frequency Modulated Guidance Laws for a Mortar Missile with a Pulse Jet Control Mechanism," *Aeronautical Journal*, Vol. 119, No. 1213, 2015, pp.389-405.
- [2] Min Gao, Yongwei Zhang, and Suochang Yang, "Firing Control Optimization of Impulse Thrusters for Trajectory Correction Projectiles," *International Journal of Aerospace Engineering*, Vol.2015, Article ID 781472, 11 pages, 2015, doi: /10.1155/2015/781472
- [3] Hollis M S L, Brandon F J, "Design and Analysis of a Fuze-Configurable Range Correction Device for an Artillery Projectile," *Report ARL-TR-2074*, U.S. Army Research Laboratory, Aberdeen Proving Ground, Aberdeen, MD, 1999.
- [4] Rogers J, Costello M, "Control Authority of a Projectile Equipped with a Controllable Internal Translating Mass," *Journal of Guidance, Control, and Dynamics*, 2008, 31(5): 1323-1333.
- [5] Rogers J, Costello M, "Design of a Roll-Stabilized Mortar Projectile with Reciprocating Canards," *Journal of Guidance, Control, and Dynamics*, Vol. 33, No. 4, 2010, pp. 1026-1034.
- [6] Yi Wang, Weidong Song, Qingwei Guo, Xieen Song, Gang Wang, "Correction Mechanism Analysis for a Class of Spin-stabilized Projectile with Fixed Canards," *Engineering Letters*, Vol. 23, No. 4, 2015, pp. 269-276.
- [7] Spagni J, Theodoulis S, Wernert P, "Flight Control for a Class of 155 mm Spin-Stabilized Projectile with Reciprocating Canards," *AIAA Guidance, Navigation, and Control Conference*, 2012
- [8] Murtaugh S A, Criel H E, "Fundamentals of Proportional Navigation," *IEEE Spectrum*, Vol. A41, 1966, pp. 75 -85.
- [9] Kim B S, Lee J G, Han H S, "Biased PNG Law for Impact Angular Constraint," *IEEE Transactions on Aerospace and Electronic Systems*, Vol. 34, No. 1, 1998, pp. 277-288.
- [10] Erer K S, Özgören M K, "Indirect Impact-Angle-Control Against Stationary Targets Using Biased Pure Proportional Navigation," *Journal of Guidance, Control, and Dynamics*, Vol. 35, No. 2, 2012, pp.700-703.
- [11] Ratnoo A, Ghose D, "Impact Angle Constrained Interception of Stationary Targets," *Journal of Guidance, Control, and Dynamics*, Vol. 31, No. 6, 2008, pp. 1816-1821.
- [12] Yongwei Zhang, Min Gao, Suochang Yang, and Dan Fang, "Optimization of Trajectory Correction Scheme for Guided Mortar Projectiles," *International Journal of Aerospace Engineering*, Vol.2015, Article ID 618458, 14 pages, 2015, doi: /10.1155/2015/618458